COMMUNICATION

The growth of porous carbon fibres through *in situ* vapour deposition

Yi'en Zhou[*a] and Liang Hong[ab]

This study investigates the transition of carbon flakes to porous carbon fibres (PCF) through vaporisation fragments of polyaromatic hydrocarbons (PAH) and their *in situ* condensation under the co-gas atmosphere of N_2 and CO_2 (v/v = 1), where CO_2 plays a vital role in cutting out vaporizable PAH fragments. The polycrystalline PCF exhibit *d*-spacings as large as 17 Å within the mesoporous framework.

As a unique form of porous carbon, porous carbon fibres (PCF) are unlike either carbon nanotubes or granular activated carbons. PCF possess different contours, sizes and most importantly, polycrystalline structures with broad ranges of *d*-spacing values as well as a mesoporous carbon framework. Chemical vapour deposition method has traditionally been used to grow carbon nanotubes[1] from CH_4 or C_2H_2 and bamboo-like carbon nanotubes on copper foils from ethanol.[2]

It has been found that fibrous activated carbons exhibit better capabilities than their granular counterparts to entrap condensable vapours,[3–6] owing to their structural traits of higher aspect ratios as well as interconnected micro- and meso-pores. Whilst long activated carbon fibres are normally produced from acrylic textile fibres and other polymer precursors through lengthy procedures,[7] short and ultrathin fibres are formed by the electrospinning technique.[8–13] In order to generate pores in a carbon matrix, carbon dioxide etching is a post carbonization treatment that engraves internal micropores without causing obvious alteration in contour to the fibres formed.[14] Alternatively, the construction of various mesoporous carbon frameworks has been carried out through the design of polymer precursors, in which using templates is a typical strategy.[15–17] Contrary to the direct transition from small organic molecules or polymers to fibrous carbons *via* carbonization and then CO_2 etching, this work unveils an alternative transition from an

activated carbon flake to a PCF structure undertaken under CO_2 and a co-gas atmosphere only. Hence, this transition differs from the transformations of carbon allotropes[18–21] because the former, in principle, involves convective mass transfer whereas the latter do not.

The initial carbon powder sample was prepared from 2-hydroxyethyl cellulose (HEC) by the method discussed elsewhere.[22] The resulting carbonaceous powder was then activated at 700 °C under CO_2 for 1 h (500 cm^3 min^{-1}) and cooled in an Ar purging stream. The activated carbon powder consisting of irregular and dense carbon flakes (Fig. 1a) was obtained thereafter through proper cleaning in water. The activated carbon powder was then heated in a tubular reactor to 800 °C under a specific gas stream (50 cm^3 min^{-1}) and this heat treatment (or incubation) lasted for 5 h (unless otherwise stated) to incubate PCF. The FESEM images (Fig. 1b and c) show clumps of the PCF developed under different incubation atmospheres resulting in different contours. The TEM image (Fig. 1d) was taken from a
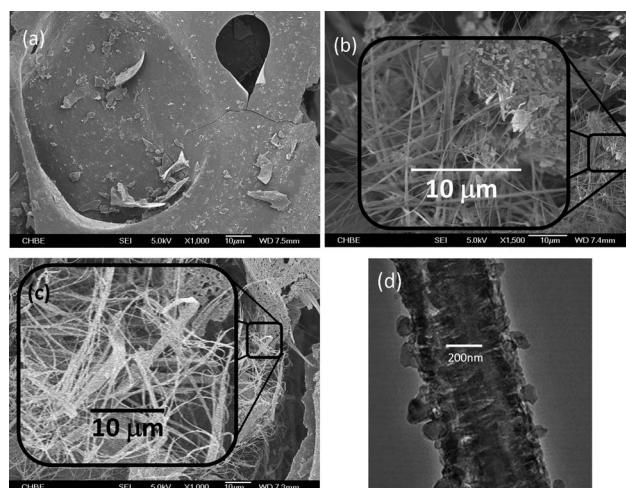
aDept of Chemical & Biomolecular Engineering, National University of Singapore, Singapore. E-mail: chezhouy@nus.edu.sg

bInstitute of Material Research Engineering, Singapore

Fig. 1 (a) Activated carbon flake; (b) pure N_2 5 h; (c) N_2–CO_2 5 h; (d) TEM image of fibre from sample 1 (c).

strand of the PCF harvested under N_2–CO_2. This fibre displays a spine-like structure assembled by sub-micron carbon wedges and interstitial voids. Although the complete mechanism of this transition has yet to be fully understood, experiments done to-date including those described in the following sections suggest that it takes place through the vaporization and *in situ* condensation of PAH fragments leading to the formation of polycrystalline carbon wedges, which subsequently assemble to form the fibres.

The microstructures of the carbon products collated from the reactor were scrutinized by electron microscopy (JSM-6700F Field Emission Scanning Electron Microscope, JEOL) whilst the porous features of the prepared PCF samples were obtained from nitrogen isotherms at 77 K by Brunauer–Emmett–Teller (BET) surface area measurement (Autosorb-1, Quantachrome instruments). Prior to each measurement, the prepared PCF samples were degassed at 300 °C for 3 h. The surface area (A_{BET}) was calculated from the linear region of the adsorption isotherm under the relative pressure (P/P_0) from 0.05 to 0.3. Crystalline characteristics of the samples were analysed on a X-ray diffractometer (Brucker D8 Advance, Cu Kα radiation $\lambda = 1.54$ Å) and the pendant organic functional groups on carbon skeleton were characterized by Fourier transform infrared spectroscopy (FT-IR) using the KBr pellet window method. Finally, the H_2S adsorption attributes of the PCF and the control samples were determined at 25 °C in a fixed bed microreactor (diameter: 10 mm; length: 200 mm) where 0.05 g of an adsorbent was packed for each measurement. A H_2S (1100 ppm)–N_2 balance stream was fed with a flow rate of 1000 cm^3 h^{-1} at 1 atm. The H_2S concentration in the outlet gas was detected by an electrochemical sensor (MOT500-H_2S, Keernuo Electronics Technology). The change in H_2S concentration in the outlet stream portrays the adsorption capacity of the testing sample. The breakthrough time is defined as the time that elapses before the bed exit-concentration of H_2S reaches 1% of the inlet concentration.

The hypothesis of flake-to-fibre transition through vaporization of PAH was verified by using a specimen of graphite powder (Sigma Aldrich) *in lieu* of the carbon flakes to conduct the fibre growth experiment under identical conditions to those used to prepare the sample in Fig. 1c. Unlike the thick PCF growth in sample 1c, only a scarce number of fibres in larger diameters can be incubated from the graphite specimen because of the strong association of graphene sheets in graphite. The occurrence of the fibres supports the etching role of CO_2 and the proposed sublimation/deposition mechanism. Fig. 2 provides a closer inspection of the micro-environment surrounding a short segment of an arbitrary fibre originating from graphite. Numerous small graphite chips display discernible rough shapes and emerge near the fibre segment on a graphite chunk. It is thus construed that these chips must be the remaining CO_2-reactive graphite pieces from the incubation process. Besides this, the nick in the selected fibre segment shows the bulk morphology of the fibre that comprises tiny strands. These strands were regarded as the product of deposition of the stripped miniature graphene pieces. Accompanying the consecutive fusion of graphene pieces, the strands
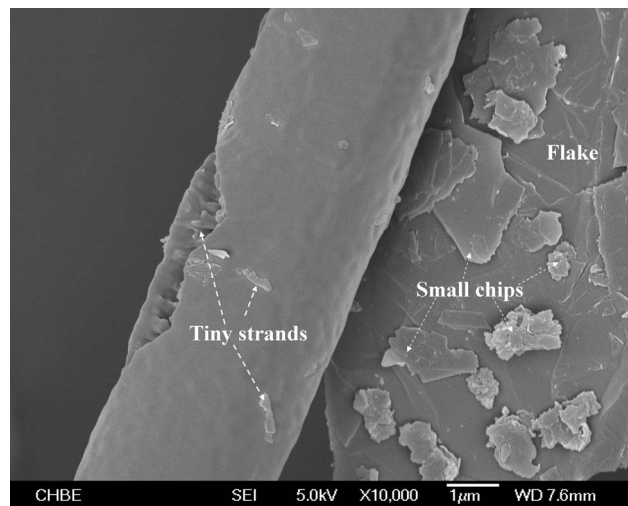

Fig. 2 Magnified view of a single fibre grown from graphite particles attached to its surface under N_2–CO_2 incubation.

gradually merged together to form scaffolds, which ultimately connected with each other to form a fibre. As it would be far more difficult to strip graphenes than PAHs from their respective carbon sources under the incubation conditions, much fewer fibres could be eventually generated from graphite. Moreover, unlike what was shown in Fig. 1d, the dense fibre matrix might arise from continuous filling of tiny graphene pieces into niches throughout the course of fibre formation. We also observed that only trace quantities of fibre strands could be generated if CO_2 was absent from the incubation atmosphere, validating the role of CO_2 in skinning miniature graphenes.

With the exception of the above control experiment, the infrared spectra of the three incubated samples obtained from different treatment conditions (Fig. 3) show clearer aromatic ring stretching peaks (close to 1500 cm^{-1} and 1600 cm^{-1}) compared to that of the activated carbon powder besides the overtone bands (1600–1800 cm^{-1}). This is due to the occurrence
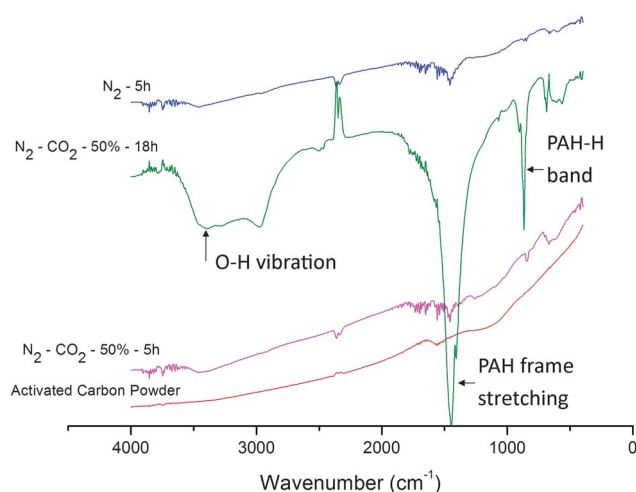

Fig. 3 FT-IR spectra showing the change in organic functional groups due to activation and incubation.

of a fraction of smaller PAH rings with similar sizes[22] as the compiling PCF. It is rational to deem that both CO_2 and thermal etchings cut up PAH rings on the surface of flakes into smaller ones, which contribute to the construction of PCF. In particular, an extension of incubation from 5 to 18 h under N_2–CO_2 gave rise to a majority of smaller PAH species, which also bear phenolic groups according to the obvious O–H vibration band (3400 cm^{-1}). Yet, the 18 h incubation left behind only a small amount of carbon residue, including negligible PCF. The reason for the depletion of PCF from this sample should be due to the fact that PCF is far reactive than the carbon flakes towards CO_2. Hence, the growth of PCF and the *in situ* etching of them shifted to the latter side with the extension of treatment, leaving behind a collection of smaller PAH with the substituted –OH group. This functional group must initially come from CO_2 through a complex conversion process since the activated carbon sample showed no oxy-group characteristics in its IR spectrum. It can also be deduced that the PAH with a high –OH substitution degree is immune to further etching by CO_2 and converted to PCF. Therefore, the residue survived from the excessively extended incubation duration.

It is also noteworthy that the activation step had created some reactive sites in the carbon flakes before the incubation treatment. It is essential to the subsequent growth of PCF. This is because the incubation step applied a delicate flow rate of CO_2 as described above in order to avert PCF formed from being destroyed by a higher CO_2 flow. In addition, the use of N_2 instead of CO_2–N_2 as the atmosphere for incubation also resulted in PCF as shown in Fig. 1c. This test shows as well the effect of the reactive sites inherited from the previous activation step. It is also clear that the PCF in Fig. 1b display straighter contours and a denser matrix compared to that in Fig. 1c. As per the observation, the thermal etching under N_2 should produce PAH fragments with more regular structure and hence, a more closely packed PCF matrix as a logical conclusion, which is further justified subsequently by BET surface analysis.

The impact of incubation atmosphere on both the conversion and pore structures in the three co-gases (N_2, He, or Ar) of CO_2 demonstrated that lesser PCF were formed in CO_2–He compared to CO_2–N_2 (Fig. 1c), whilst almost no PCF were obtained (with most of the initial carbon flakes remaining intact) when the transition was conducted in CO_2–Ar. This fact suggests that the co-gas would have affected the activity of CO_2. This observation may be explained using the pre-exponential factor A of bi-molecular collision model[23] since it reflects collision effectiveness at a given temperature:

$$A = \frac{1}{4} N_A \pi \left(d_i + d_j\right)^2 \left[\frac{8RT}{\pi}\left(\frac{M_i + M_j}{M_i M_j}\right)\right]^{\frac{1}{2}} e^{0.5}$$

where the subscript i and j represent two molecules; symbol d and M represent molecular diameter and molecular weight respectively. The cross A values show the order $A(CO_2$–He$) > A(CO_2$–$N_2) > A(CO_2$–Ar$)$ while the A values of same kind ($i = j$) are trivial in comparison. In principle, a greater A value will lead to more frequent intermolecular collisions and hence, impede the probability of the gas molecules landing onto carbon surfaces.

On the other hand, the competitive adsorption onto the carbon surface by each individual co-gas against CO_2 (330 pm) should follow their kinetic diameters,[24] which is N_2 (364 pm) > Ar (340 pm) > He (260 pm). It is therefore considered that the CO_2–N_2 combination trades off these two factors, granting CO_2 highest touchdown frequency to the carbon flakes. Similarly, a change in the CO_2 concentration in N_2 from 50% to either 90% or 10% produced fewer fibres due to an over or insufficient etching extent.

During the condensation process, a coaxial stacking of submicron carbon wedges that consists of the planar PAH molecules takes place (Fig. 1d). This hierarchy is verified by the X-ray diffraction results (Fig. 4). Against an amorphous structure displayed by the activated carbon flakes, the products from the incubation under the three different atmospheres (*i.e.* N_2, CO_2–N_2, and CO_2–He) display different polycrystalline structures as a result of multiple randomised stacking of PAH molecular fragments different in sizes and with oxy-groups attached. It is noted that the PCF incubated under N_2 (or He)–CO_2 displays a very broad coverage of d-spacing, ranging from 17.9 Å to a mere 0.91 Å. Thus, the PCF offer far greater distances between PAH sheets than normal graphitized carbon adsorbents that have the inter-graphene distance of 3.35 Å.[25] As noted above, the residue of the 18 h incubation under N_2–CO_2 is prevalently amorphous phase due to the diminution of the majority of PCF. A conclusion can thus be drawn from the above X-ray characterization: it was the PCF rather than the activated carbon source that contributed to the crystalline features despite the difficulty in separating PCF from the carbon residue as both were entangled together. As such, the intensity of crystalline peaks could approximate the relative content of PCF in a sample. Indeed, similar conversions of the activated carbon flakes to PCF were attained under the He–CO_2 and N_2–CO_2 streams, respectively.

Although there was difficulty in separating the PCF from the flakes, close examination under electron microscopy shows that
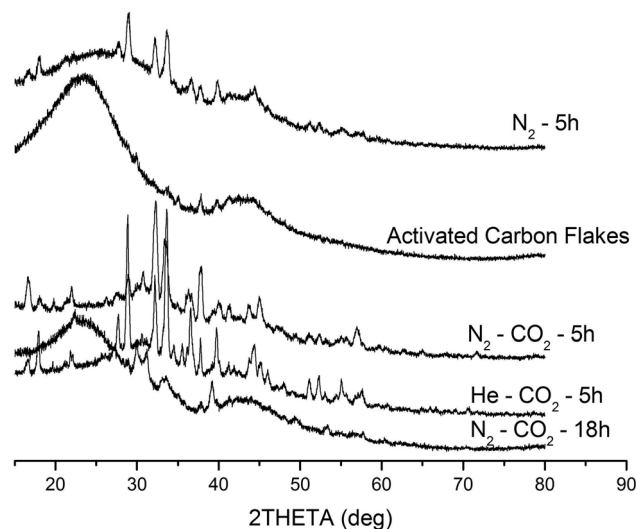

Fig. 4 X-ray diffraction results.

both the He–CO_2 and N_2–CO_2 streams produced a conversion of *ca.* 40% to fibres by volume (40% yield) whilst conversion under Ar–CO_2 stream produced no PCF (0% yield). A mass loss of *ca.* 20% was also observed in all samples regardless of the incubation atmosphere. In addition, as mentioned previously, CO_2 plays a major role in this transition and the yield drops significantly to *ca.* 15% when CO_2 was not included in the treatment during the incubation. The incubation duration, the identity of co-gas, and the flow rate of CO_2 are the key factors affecting the yield of PCF at the selected incubation temperature, which have been elucidated in the preceding paragraphs.

As far as the porous structures evolved under different atmospheres are concerned, their BET isotherms and the specific surface properties are ostensibly greater than that of the activated carbon flakes specimen, which exhibits a feeble microporous structure with the most abundant pore size of 16 Å (0.24 cm^3 g^{-1}) and a specific surface area of 250 m^2 g^{-1}. When it is incubated under N_2, the pure thermal etching triggers formation of mesoporosity ($v_m/v_t = 0.66$). It is in accordance to its lower 2θ XRD peaks together with an increase in surface area. Furthermore, a change of the incubation atmosphere to N_2–CO_2 permits CO_2-etching and hence, resulting in an even greater harvest of PCF. This contributes towards the mesoporosity ($v_m/v_t = 0.68$), the total specific pore volume (0.81 cm^3 g^{-1}) and the surface area (1140 m^2 g^{-1}). As aforementioned, if the incubation was extended to 18 h under the same atmosphere, only the phenolic PAH remained and showed a low surface area of 131 m^2 g^{-1} with a slightly increased mesoporosity ($v_m/v_t = 0.73$) but a v_t of 0.10 cm^3 g^{-1}. This outcome supports the previous inference for the occurrence of small PAH with similar ring sizes on the basis of the FT-IR spectrum since these PAH rings favour closely packing. In addition, the use of He–CO_2 as incubation atmosphere instead of N_2–CO_2 demonstrated the modest surface properties but a high mesoporosity ($v_m/v_t = 0.80$). Such effect can be presumed to be caused by the active collisions between CO_2 by He molecules, which made CO_2 could adsorb only those reactive carbon sites. With the CO_2 etching role, these sites become micro-pores and more preferential to CO_2 and hence the micro-pores were expanded to mesopores. The absorption of H_2S to the three selected specimens showed different breakthrough durations on the basis of per gram adsorbent: 1.4 min (AC-flake); 14.2 min (CO_2–N_2), 23.4 min (CO_2–He), which is in accord with the volume fraction of mesopores (v_m/v_t) (Fig. 5).

In conclusion, we have observed and described the phenomenon that a specific type of activated carbon flakes undergoes a sublimation-like process to transform to fibrous structures under a CO_2-containing binary atmosphere at 800 °C. This C-to-C transition leads to fibrous activated carbon with sizes between carbon nanotube and carbon fibre and a micro to meso porous structure. The co-gas of CO_2 plays a vital role in shaping the evolution of the activated fibre and, in particular, its porous structure. This phenomenon is presumed to originate from the different molecular collision efficiencies and the kinetic diameters of gases. Finally, the H_2S adsorption test was undertaken to validate the surface properties obtained from BET analysis.
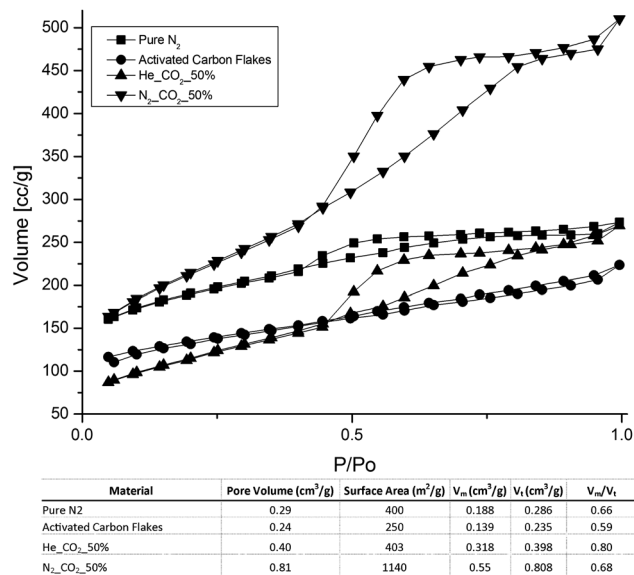

Material	Pore Volume (cm^3/g)	Surface Area (m^2/g)	V_m (cm^3/g)	V_t (cm^3/g)	V_m/V_t
Pure N2	0.29	400	0.188	0.286	0.66
Activated Carbon Flakes	0.24	250	0.139	0.235	0.59
He_CO2_50%	0.40	403	0.318	0.398	0.80
N2_CO2_50%	0.81	1140	0.55	0.808	0.68

Fig. 5 Isotherms of BET for various pore structures.

Notes and references

1 H.-C. Lin, S.-T. Shiue, Y.-H. Cheng, T.-J. Yang, T.-C. Wu and H.-Y. Lin, *Carbon*, 2007, **45**, 2004–2010.

2 J. T. Zhu, J. C. Jia, F. L. Kwong and D. H. L. Ng, *Carbon*, 2012, **50**, 2504–2512.

3 E. A. Dawson, G. M. B. Parkes, P. A. Barnes, M. J. Chinn, L. A. Pears and C. J. Hindmarsh, *Carbon*, 2002, **40**, 2897–2903.

4 M. Suzuki, *Carbon*, 1994, **32**, 577–586.

5 Y. K. Zhan, C. Y. Nie, H. B. Li, L. K. Pan and Z. Sun, *Electrochim. Acta*, 2011, **56**, 3164–3169.

6 J. Y. Zhou, Z. W. Wang, R. Zuo, Y. Zhou, X. M. Cao and K. Cheng, *Asia-Pac. J. Chem. Eng.*, 2012, **7**, S245–S252.

7 P. J. M. Carrott, J. M. V. Nabais, M. M. L. Ribeiro Carrott and J. A. Pajares, *Carbon*, 2001, **39**, 1543–1555.

8 M. Aceituno-Medina, A. Lopez-Rubio, S. Mendoza and J. M. Lagaron, *Food Hydrocolloids*, 2013, **31**, 289–298.

9 S. Agarwal, A. Greiner and J. H. Wendorff, *Prog. Polym. Sci.*, 2013, **38**, 963–991.

10 T. Maitra, S. Sharma, A. Srivastava, Y.-K. Cho, M. Madou and A. Sharma, *Carbon*, 2012, **50**, 1753–1761.

11 Y. Qiu, J. Yu, T. Shi, X. Zhou, X. Bai and J. Y. Huang, *J. Power Sources*, 2011, **196**, 9862–9867.

12 X. Song, Z. Wang, Z. Li and C. Wang, *J. Colloid Interface Sci.*, 2008, **327**, 388–392.

13 A. Greiner and J. H. Wendorff, *Angew. Chem., Int. Ed.*, 2007, **46**, 5670–5703.

14 J. Alcañiz-Monge, D. Cazorla-Amorós, A. Linares-Solano, S. Yoshida and A. Oya, *Carbon*, 1994, **32**, 1277–1283.

15 D. Gunther, J. Beckmann, M. Schoneich, P. Schmidt and O. Klepel, *Carbon*, 2012, **50**, 3096–3098.

16 S. Lei, J. I. Miyamoto, T. Ohba, H. Kanoh and K. Kaneko, *J. Phys. Chem. C*, 2007, **111**, 2459–2464.

17 Y. Meng, D. Gu, F. Q. Zhang, Y. F. Shi, H. F. Yang, Z. Li, C. Z. Yu, B. Tu and D. Y. Zhao, *Angew. Chem., Int. Ed.*, 2005, **44**, 7053–7059.

18 C. He, L. Z. Sun and J. Zhong, *Journal of Superhard Materials*, 2012, **34**, 386–399.

19 F. P. Bundy, W. A. Bassett, M. S. Weathers, R. J. Hemley, H. K. Mao and A. F. Goncharov, *Carbon*, 1996, **34**, 141–153.

20 V. V. Brazhkin, A. G. Lyapin, S. V. Popova, S. C. Bayliss, T. D. Varfolomeeva, R. N. Voloshin, A. G. Gavrilyuk, M. V. Kondrin, V. V. Mukhamad'yarov, I. A. Troyan, S. V. Demishev, A. A. Pronin and N. E. Sluchanko, *JETP Lett.*, 2002, **76**, 681–692.

21 K. Yamada, Y. Tanabe and A. B. Sawaoka, *Philos. Mag. A*, 2000, **80**, 1811–1828.

22 M. Sun and L. Hong, *Carbon*, 2011, **49**, 2173–2180.

23 P. W. Atkins, *Atkins' physical chemistry*, Oxford University Press, Oxford, New York, 2006.

24 G. Aguilar-Armenta, G. Hernandez-Ramirez, E. Flores-Loyola, A. Ugarte-Castaneda, R. Silva-Gonzalez, C. Tabares-Munoz, A. Jimenez-Lopez and E. Rodriguez-Castellon, *J. Phys. Chem. B*, 2001, **105**, 1313–1319.

25 C. G. Zoski, *Handbook of Electrochemistry*, Elsevier Science, 2007.